Comparative study of porous iron electrodes

J. Černý
Mládežnická 1270, 293 01 Mladá Boleslav (Czech Republic)

J. Jindra and K. Micka*
J. Heyrovský Institute of Physical Chemistry, Czech Academy of Sciences, 182 23 Prague 8 (Czech Republic)

(Received December 29, 1992; accepted in revised form February 27, 1993)

Abstract

Sintered porous iron electrodes prepared from various materials were tested and compared with similar electrodes from different manufacturers. The important role of sulfide ions as activating agent was substantiated. A common feature of the electrodes under study is a relatively high rate of self-discharge, which can only partly be attributed to the presence of impurities, mainly manganese, in the active material and/or in the current collector.

Introduction

An increasing interest has been devoted in recent years to rechargeable (porous) iron electrodes [1–3]. Iron electrodes are suitable for applications in traction batteries, since they have a high theoretical capacity (0.96 Ah per 1 g of Fe), long cycle life, and good resistance against mechanical shocks, vibrations, overcharge, and deep discharge.

Sintered iron electrodes enable the construction of accumulators for high-rate discharge and high energy density [4–11]. Very good electrodes of this type were developed by Andersson *et al.* [5–7], who made use of the double porosity concept. Laboratory sintered iron electrodes have recently been investigated by Muralidharan and coworkers [12–14], who used unusually high sintering temperatures (up to 950 °C). The sintering process was carefully studied by Bryant [15], who found that with increasing duration of sintering at 700 °C the discharge capacity of the porous iron electrode rised during the first 1 to 2 h as interconnections between iron particles were formed, and then it decreased as the specific surface area also decreased. The latter effect prevailed at temperatures around 800 °C or higher, which was also apparent from the low charge delivered by the electrodes [12, 13].

Based on these findings, the preparation and properties of sintered iron electrodes were studied in the present work and a comparison was made with iron electrodes prepared in other laboratories.

Experimental

Preparation of electrodes

Laboratory electrodes of 4 cm×7.5 cm and a thickness of 1.1–1.3 mm were prepared by pressing iron powder ('iron sponge') on to a steel mesh (from both sides) at 40 MPa and sintering in hydrogen atmosphere at temperatures up to 785 °C.

*Author to whom correspondence should be addressed.

0378-7753/93/$6.00

Powdered NaCl with particle sizes from 20 to 40 μm was used as a pore-forming agent (20–30% by weight). The starting materials for the preparation of iron sponge were the black pigment 'Fepren B 91' (Chemical Works Přerov, Czech Republic), consisting of Fe_3O_4 and the reddish-brown α-Fe_2O_3 'Bayferrox WF 1352' (Bayer, Leverkusen, Germany). The latter was also used as a pore-forming agent in some cases. The content of impurities, determined by chemical analysis, approximated 0.03% Mn and 1.2% S in Fepren, and $\leqslant$0.02% Mn, 0.05% S and 0.026% Al in Bayferrox. The manganese content is sufficiently low; the content of sulfur is favourable for a good functioning of the electrodes.

For comparison, iron sponge was also prepared from spectrally pure carbonyl iron powder, which was dissolved in dilute HCl, precipitated with KOH, washed, dried, and reduced in the same way as the other oxides.

The conditions for the reduction of the oxides in H_2 atmosphere in an oven must be chosen so that the product has a good electrical conductivity (i.e., contains mostly iron in the metallic state) and a low bulk density (up to 0.8 g/cm^3). We used temperatures of 550 to 650 °C and a reduction time of 2 to 3.5 h (the maximum thickness of the layer of the material during reduction was 2 cm). After reduction, the material was cooled (under H_2) and air was allowed to diffuse slowly into the retort for about 10 h which made the product nonpyrophoric.

The optimum temperature and the sintering time depend on the quality of the iron sponge, the arrangement of the electrodes in the retort, and the H_2 flow rate. The time necessary for attaining the sintering temperature and afterwards for cooling the retort may also play a role. Electrodes sintered for 30 min at 785 °C showed a considerable contraction and cracks, whereas those sintered for 20 min at 740 °C showed only a small contraction and their discharge capacity was 30 to 40% C_t (C_t, theoretical capacity, corresponding to 0.96 Ah per 1 g of Fe); the electrodes sintered for 20 min at 700 °C disintegrated slowly during cycling and their capacity decreased from 39 to 45% C_t in the first cycle to 20 to 27% C_t in the seventh cycle.

The iron mesh, serving as a current collector, must be sufficiently thin and the void area should be at least 60% of the geometric area, otherwise the sintered electrode may spontaneously separate into two halves.

Selected electrodes were subjected to measurements and cycle-life tests [16]; the characteristics of some of the tests (denoted as SHI) are given in Table 1. For comparison, the following electrodes from other laboratories were also tested:

(i) commercial sintered iron electrodes (denoted as SS) from the firm SAB NIFE, Oskarshamm, Sweden, 0.8 mm thick, with double porosity [5] and thin stretch metal current collector;

TABLE 1

Conditions for preparation of electrodes from iron sponge

Starting material	Reduction in H_2		Sintering in H_2		Symbol
	(°C)	(h)	(°C)	(min)	
Fepren B-91	530	5	730	40	SHI-1
Bayferrox	550	7	730–760	40	SHI-2
Bayferrox	500	8	680	90	SHI-3
Carbonyl Fe[a]	600	5	730–750	40	SHI-4

[a]See Experimental, page 267.

(ii) commercial rolled iron electrodes (denoted as RR) from the All-Union Research Designing Accumulator Institute, St. Petersburg, Russian Federation, prepared by oxidation of pure powdered iron to magnetite, reduction with hydrogen to iron sponge, and rolling on to a steel mesh [17];

(iii) electrodes from the Electrotechnical Research Institute (VKI) Budapest, Hungary, (denoted as PB-VKI), prepared by rolling a wetted mixture of iron sponge, magnetite, Na_2S, polytetrafluoroethylene (PTFE), and a carbon material on to a steel mesh;

(iv) pocket-type electrodes from the Department of Electrotechnology, Technical University, Brno, Czech Republic, (denoted as L-VUT), containing an active material FENA [18], whose basic component is the iron oxide 'polishing black' [19] treated by an activating process, and

(v) plastic-bonded laboratory electrodes from the same work place (denoted as PB-VUT), prepared by pasting a mixture of the polishing black with 5% acetylene black and 5% powdered poly(phenylene oxide), wetted with a 9:1 mixture of perchloroethylene and petrol, on to an iron mesh.

As far as possible, the tested electrodes were cut to a surface area of 4 cm × 7.5 cm.

Determination of electrochemical characteristics

The porous iron electrodes were assembled in cells with two positive pocket-type nickel hydroxide electrodes (with excess capacity) and without a separator. The electrolyte was a solution of 5 M KOH. A Hg/HgO reference electrode in 5 M KOH was used. The electrodes were discharged and charged galvanostatically at the laboratory temperature (24–26 °C). The charging was finished as soon as the potential of the iron electrode was constant for 2 h; the charge consumed was at least 250% of the charge delivered at a current density of 3 to 7 mA/cm^2 of the two-side electrode area. The discharging was finished mostly after the first step (Fe → Fe(II)), distinguished by an inflection on the E–t curve. Occasional discharging to the second step (Fe(II) → Fe(III)) at 3 to 30 mA/cm^2 was stopped at a potential of −0.3 V. The charging was started after a break of 30 to 60 min. The same discharge current of 400 mA (6.67 mA/cm^2) was used, as a rule, when the various electrodes were compared. The results are given as a percentage of the theoretical capacity, C_t, which corresponds to the reaction Fe → Fe(II).

The internal resistance was measured by the pulse method, the electrodes being loaded for 5 s with a current increasing in steps at 10 min intervals. The value of the internal resistance was obtained from the volt/ampere discharge characteristics.

The cycle life of the iron electrodes was determined in the following regime: charging at 400 mA for 4 h, discharging at 450 mA for 2 h; measuring cycle: charging at 300 mA for 16 h, discharging at 400 mA to the end of the first step.

The self-discharge of the iron electrodes was determined according to the Czechoslovakian standard 364 350.

Cyclic voltammetry on porous iron electrodes

The electrodes were placed in a prismatic cell connected with a Hg/HgO reference electrode filled with 5 M KOH. The tip of the Luggin capillary reached to the upper edge of the working electrode. A high-power potentiostat (2.5 V/60 A) with a triangular voltage source was used; the sweep rate was 2 or 10 mV/s. At higher rates, the peak separation was poor. One hour before the measurement, the working electrode was charged with a current of 150 mA.

Determination of physical parameters

The porosimetric curves and the total porosity were measured on a high-pressure mercury porosimeter type 65-4 (Carlo–Erba, Italy) in the range of pore radii from 7.5 to 0.0075 μm. The inner surface area of the iron active material was determined by the BET method on a Digisorb Z 600 apparatus (Micromeritics, USA) using nitrogen or krypton.

Results and discussion

Voltammetry

Sintered electrodes SS and SHI and rolled electrodes RR were used in this experiment; a good separation of the peaks was achieved at a sweep rate of 2 mV/s (Fig. 1). Well-developed anodic peaks are observed at -0.6 V (A_2) and at -0.4 V (A_3). With electrodes SHI and RR, peak A_3 is somewhat larger than A_2, but with electrode SS the two peaks are equal. The cathodic branch shows only slightly discernible peaks C_1 and C_2 for electrode SS at -0.95 and -1.1 V, whereas the electrodes RR and SHI show only humps in the corresponding potential regions. The higher performance of the sintered electrodes compared with the rolled ones is manifested by the differences between the peak heights.

Similar voltammograms were obtained by Kalaignan *et al.* [12], the anodic peaks being somewhat shifted to more negative potentials. However, their maximum current densities were substantially lower, which is probably caused by the appreciably higher sintering temperature used.

Andersson and Öjefors [20] recorded voltammograms for an iron electrode prepared according to the method by Lindström [4]. They obtained two anodic and two cathodic peaks at potentials corresponding to the steps on the galvanostatic E–t curves: A_2 at -0.8 V, A_3 at -0.63_5 V, C_1 at -1.01 V, and C_2 at -1.2 V. The anodic peak potentials found in our laboratory are less negative owing to the higher sweep rate (2 mV/s); at a sweep rate of 10 mV/s still less negative peak potentials were measured (A_2 at -0.58 V, A_3 at -0.1 V; C_1 at -0.98 V was only little affected).

Peak A_2 probably corresponds to the oxidation of Fe(0) to Fe(II) (first step) and A_3 to the oxidation of Fe(II) to Fe(III) (second step). It can be assumed [21] that the latter involves also the oxidation of Fe(0) to Fe(III). The cathodic peak C_1 is the reverse of A_3, and C_2 is the reverse of A_2. At sweep rates higher than 5 mV/s, these peaks are only slightly discernible and the cathodic branch of the curve passes smoothly into the region of H_2 evolution.

Except for electrodes with starting material the sulfur-containing oxide Fepren, an at least two-fold increase of peak A_3 was observed after addition of Na_2S into the solution (in final concentration of 0.01 M), but in subsequent cycles the peak decreased. The decrease was only slight with electrode SS, moderate with SHI, and considerable with RR. At the same time, shedding of the active material from the latter two electrodes was observed, probably owing to deep discharges with a polarity reversion to positive potentials (Fig. 1). No such effect was observed with the electrode SS. It appears that cyclic voltammetry can serve as a rapid method for judging the adhesion between the active material and the current collector, which limits the cycle life of the electrode (see below, Cycle-life tests).

A substantial increase of the anodic peak after addition of Na_2S into the electrolyte was also observed by Kalaignan *et al.* [12]. Sulfide ions effectively suppress the formation

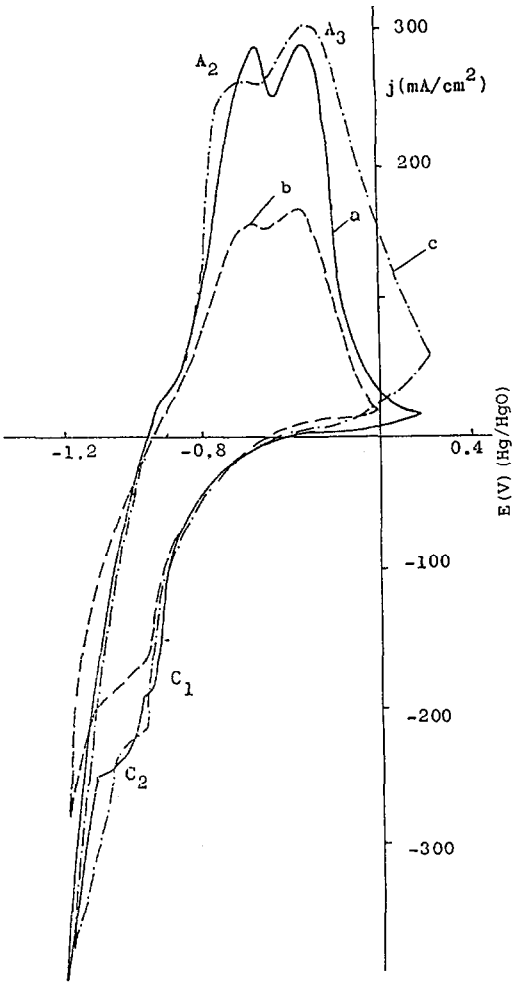

Fig. 1. Voltammograms for porous iron electrodes; sweep rate 2 mV/s, third cycle. (a) Electrode SS; (b) electrode RR, and (c) electrode SHI-4.

of anodic passive layers. On deep discharge of the iron electrode with potential reversal, sulfide ions are oxidized and the electrode may passivate again, unless it contains sulfur built-in in the solid phase, as, e.g., the electrodes prepared from Fepren.

Galvanostatic E–t curves

E–t curves for the test electrodes during discharge are shown in Fig. 2. With electrode SS, the *E–t* curve is the best developed, the potentials of the two discharge steps are nearly constant and the length of the first discharge step is twice that of the second one, evidence for the good utilization of the active material. The curves for electrodes SHI and RR are similar. The other electrodes (PB-VKI, PB-VUT, and L-VUT) have either a lower capacity or their potential decreases with the charge delivered.

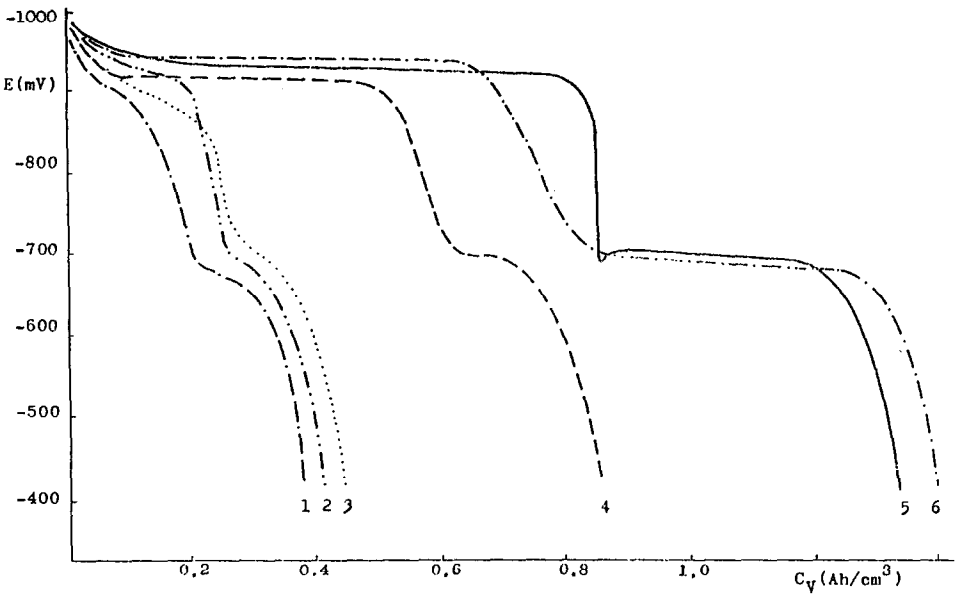

Fig. 2. Discharge curves for porous iron electrodes; current density $j=6.67$ mA/cm^2, 10th cycle. Curve (1) electrode L-VUT; curve (2) PB-VKI; curve (3) PB-VUT; curve (4) RR; curve (5) SS, and curve (6) SHI.

From the point of view of the capacity, the sintered electrodes SS and SHI appear preferable, since they can be made relatively thin (roughly 1 mm), which is not possible with the other electrodes in view of their limited mechanical strength.

The capacity of the electrodes prepared from Fepren as starting material was independent of the addition of Na_2S, since sulfur was built-in in the active material. With the electrodes prepared from spectrally pure iron, however, the capacity in the pure electrolyte was determined as 26% C_t in the first cycle and it dropped gradually to as low as 2% C_t in subsequent cycles; a normal behaviour was restored by adding Na_2S into the electrolyte (at a final concentration of 0.01 M), resulting in 35% C_t. Thus, it can be concluded that traces of sulfur are indispensable for a proper functioning of the iron electrode.

The data on capacities, iron content, and other parameters of the iron electrodes are summarized in Table 2.

Charging curves (Fig. 3) were measured at current densities $j_n=5$ and 13 mA/cm^2 (referred to both sides) with electrodes SS, SHI, RR, and PB-VUT after they had been discharged to the second step, i.e., to -0.3 V. The electrode capacity was almost independent of the charging current used (the measured values were 47 and 49% C_t for electrode SS, 23 and 22% for RR, 41% for SHI, and 36% for PB-VUT, respectively). The potential delays corresponding to the charging steps are the best developed with electrodes SS and SHI: the reduction of Fe(III) to Fe(II) proceeds in the potential region from -0.9 to -1.0 V (at the higher current density), the reduction of Fe(II) to Fe(0) in the region from -1.05 to -1.15 V, and the evolution of H_2 prevails beginning from -1.25 V.

The charging steps are less distinguished with thicker electrodes (RR), probably as a result of the current distribution in the depth of the pores.

TABLE 2

Parameters of the iron electrodes: d, thickness; ρ, bulk density of electrode; ρ_a, bulk density of active mass; C_t, theoretical capacity; C_a, actual capacity; C_m, mass specific capacity; R_i, internal resistance

	SS	SHI-1	SHI-2	SHI-3	SHI-4	RR	PB-VKI	PB-VUT	L-VUT
d (mm)	0.8	1.1	1.1	1.1	1.1	1.6	2.5	1.9	2.0
ρ (g/cm^3)	3.13	2.87	2.91	3.02	2.91	3.63	2.50	2.16	5.30
ρ_a (g/cm^3)	2.13	1.82	1.82	1.83	1.82	2.88	2.32	1.45	1.45
% of Fe	88	93	93	93	93	82	66	59	55
g of Fe	4.5	5.6	5.6	5.6	5.6	11.3	11.4	4.1	4.8
C_t (Ah)	4.3	5.4	5.4	5.4	5.4	10.8	10.9	3.9	4.6
C_a (Ah)	2.65	1.8	2.25	2.40	2.02	2.65	1.75	1.40	1.0
C_a/C_t (%)	48	33	42	45	37	25	16	36	22
C_m (Ah/g)	0.27	0.1	0.23	0.25	0.21	0.15	0.08	0.11	0.03
R_i (mΩ)	27	35	35	35	35	35	40	42	66

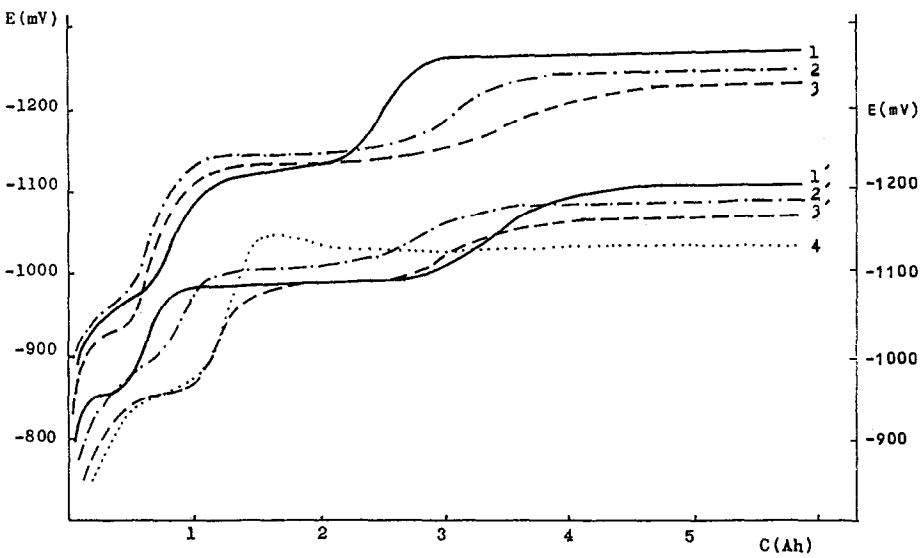

Fig. 3. Charging curves for porous iron electrodes; left potential axis: $j = 13.3$ mA/cm^2; right potential axis: $j = 5$ mA/cm^2; 10th cycle. Curves (1,1') electrode SS; curves (2,2') SHI; curves (3,3') RR, and curve (4) PB-VUT.

With the plastic-bonded electrode PB-VUT, the first charging step (Fig. 3) coincides with the evolution of H_2, resulting in a lower charging efficiency. Similar charging curves were obtained with electrodes PB-VKI and L-VUT.

Generally, the potential of the charging step is at the usual current densities (above 3 mA/cm^2) more negative than the equilibrium potential of H_2 evolution, -0.975 V, so H_2 is evolved already from the beginning of charging if the electrode was discharged only to the first step (i.e., almost always, since discharge to the second step is unusual).

Internal resistance

Internal resistances of the electrodes under study are given in Table 2. The smallest value corresponds to the electrode SS (sintered under pressure), which has a small thickness and a hard consistency. Somewhat higher values for the electrodes RR (rolled) and SHI (sintered without pressure) are probably due to their higher thickness and to a contact resistance between the active material and the current collector. As expected, elevated internal resistance was found with the electrodes PB-VKI and PB-VUT, owing to the presence of the nonconducting plastic binder. High internal resistance of the pocket-type electrodes L-VUT is due to their construction.

Self-discharge

The self-discharge of the iron electrodes in the pure electrolyte was in the range of 9 to 29% after 2 days and of 36 to 64% after 10 days (Table 3). Its rate was always higher during the first days of the test, after which it decreased gradually. Differences between the self-discharge rates may be attributed to the effect of trace impurities in the materials used, mainly manganese (in all samples), and in the current collectors. Thus, the low self-discharge of the electrode SS is most probably due to the pure-iron stretch metal used as current collector, and to the pure starting material. The same starting material used with an ordinary iron mesh (electrodes SHI-2 and SHI-3) had a higher self-discharge, which increased further when Fepren B 91 with a higher manganese content was used (see Experimental). The self-discharge of electrode SHI-4 from spectrally-pure iron is presumably partly due to the ordinary iron mesh current collector. Naturally, the insufficient separation of the equilibrium potential of the iron electrode from the potential of H_2 evolution plays a significant role.

The rate of self-discharge was unaltered in the presence of 0.04 M Na_2S in the electrolyte, although Öjefors [22] recommended the addition of K_2S to lower the rate of self-discharge. Addition of tartaric acid (1.5 g per 100 ml), recommended for the same purpose by some authors [22, 23], caused disintegration of our sintered electrodes during cycling owing to the formation of a soluble iron complex.

With respect to previous work [21, 23], it was of interest to determine the effect of selenium and tellurium on the self-discharge. We used additions of 0.01 and 0.1 g of SeO_2 or H_6TeO_6 per l of electrolyte. Whereas the self-discharge rate of electrode SS was unchanged by the additions of SeO_2, there was a threefold increase

TABLE 3

Self-discharge (loss of capacity measured at 6.67 mA/cm^2) of the iron electrodes

Electrode	Starting material	Self-discharge in % after	
		2 days	10 days
SS	Bayferrox WF 1352	9	36
RR	Synthetic magnetite	16	50
SHI-1	Fepren B 91	29	64
SHI-2	Bayferrox WF 1352	13	53
SHI-3	Bayferrox WF 1352	11	50
SHI-4	Carbonyl iron	10	45
PB-VKI	Synthetic Fe_2O_3	22	54
PB-VUT	Polishing black	20	50
L-VUT	Polishing black	14	45

in the electrolyte containing tellurate ions. Tellurium is apparently deposited on the negative iron electrode, causing a decrease of the H_2 overpotential. An analogous effect takes place on lead electrodes in acid solutions [24, 25]. Nevertheless, Mitsumata and Iwaki [23] recommended the addition of TeO_2 into the electrolyte to increase the charging efficiency of their iron electrodes.

Cycle-life tests

The results of cycle life tests of the studied electrodes are shown in Fig. 4. A sufficient cycle life was attained with electrodes SS, SHI-3, and RR. The latter showed a gradual increase of the capacity with a maximum in the range from 300 to 600 cycles. A similar observation was made by Vijayamohanan *et al.* [26] with pressed electrodes from iron sponge and polyethylene. Apparently more and more particles become involved in the current generation.

No shedding of active material was observed with electrodes SS, RR, and PB-VKI. The end of life of RR and PB-VKI is probably due to a gradual loss of contact between particles of the active material, caused by volume changes during cycling (see below). The drop in capacity of the electrodes SHI was caused by disintegration of the active material.

Structural parameters of the iron electrodes

Porosimetric curves of some electrodes are shown in Fig. 5. They were used to determine the specific volumes, V_{58} and $V_{7.5}$ (cm^3/g), of pores with radii up to 58 and 7.5 μm, respectively, and the volume porosities, V_{58} and $V_{7.5}$, based on the apparent

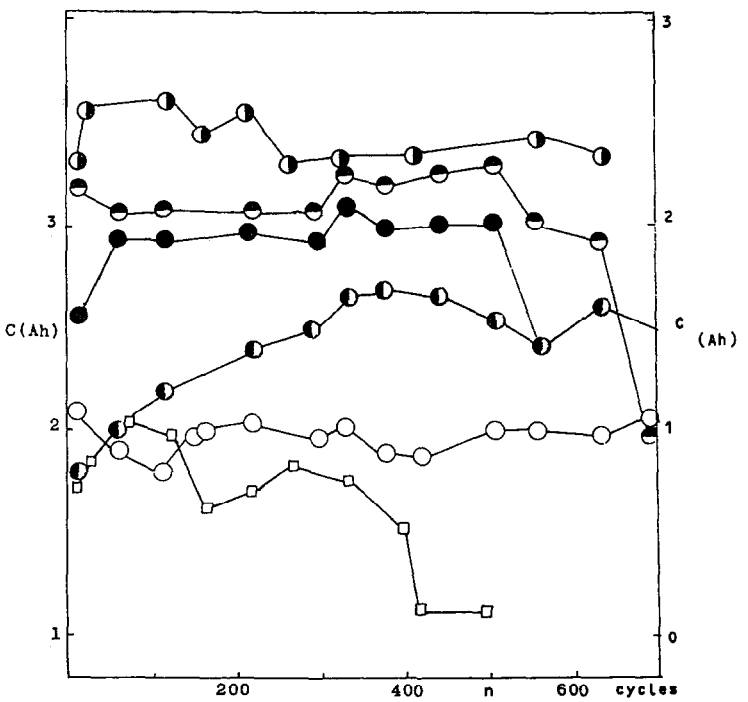

Fig. 4. Cycle-life tests (capacity as function of the cycle number). Right axis: (◓) SHI-2; (◑) SHI-3, and (●) SHI-4; left axis: (◐) RR; (○) SS, and (□) PB-VKI.

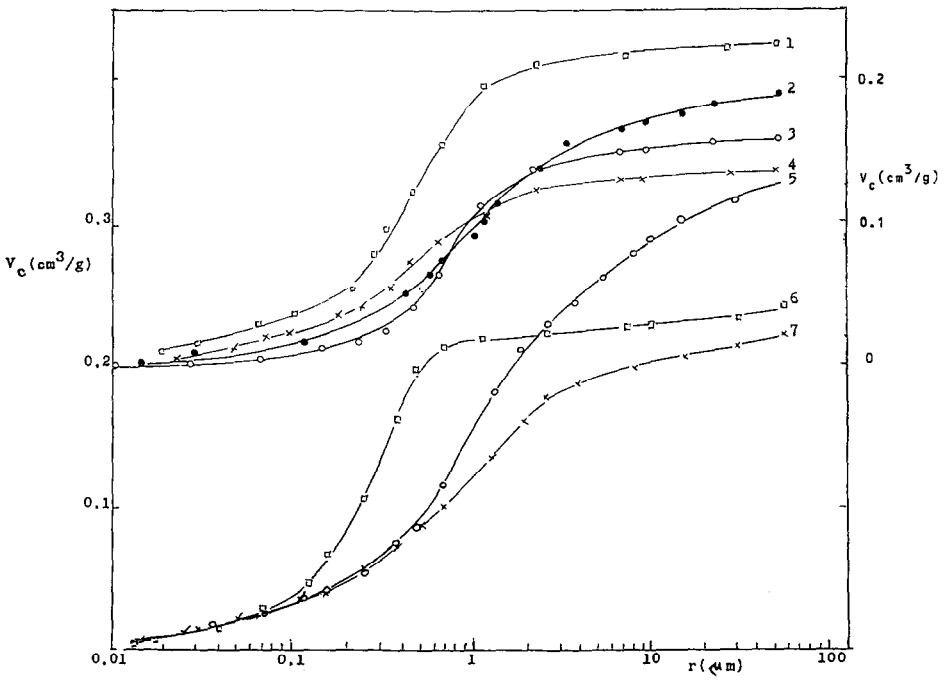

Fig. 5. Porosimetric curves: (1) electrode SS after cycling; (2) RR after cycling; (3) RR before cycling; (4) SS before cycling; (5) SHI-4 after cycling; (6) SHI-3 after cycling, and (7) SHI-3 before cycling. Left scale refers to electrodes SHI-3 and SHI-4, right scale to SS and RR.

densities (Table 2). The specific surface area of pores, S (m^2/g), and the radius of pores with maximum abundance, r_{max}, were estimated from the porosimetric curves on the assumption that the pores are cylindrical, see Table 4.

The occurrence of pores with radii from 2 to 50 μm in electrodes SHI is due to the filler (NaCl), which has been washed out, and possibly to the formation of microscopic cracks during sintering. A general feature is the increase of the pore volume and pore radius with cycling. This may limit the cycle life.

The highest value of the specific (BET) surface area was found with the electrode PB-VKI. This can be attributed to the 10% carbon level in the active mass. The values for the sintered electrodes were in the range of 5 to 9 m^2/g, and in good agreement with published data [15]. A surprising value, only 0.93 m^2/g, was found with the noncycled electrode RR, although the measurement was repeated when either nitrogen or krypton was used. After the cycle-life test, however, the surface area increased more than tenfold. The large difference between the surface areas of noncycled SS and RR electrodes may be, at least, partly attributed to the different forms of the iron particles. The increase in surface area of the RR electrode during cycling is favourable to its discharge capacity.

SEM microphotographs

The electrodes SS (Fig. 6(a)) have a distinct double structure [5]: the sintered agglomerates of the iron sponge have a microstructure (consisting of 0.1–1 μm particles), which is interrupted by cracks, whose borders are formed by a continuous, apparently

TABLE 4

Results of porosimetric measurements of the iron electrodes and their BET specific surface area

Electrode	$V_{7.5}$ (cm^3/g)	V_{58} (cm^3/g)	$\bar{V}_{7.5}$ (%)	$\bar{V}_{58}$ (%)	r_{max} (μm)	S (m^2/g)	S_{BET} (m^2/g)
SS new				68[a]	0.3–0.8	3.3	11.0
SS cycled	0.221	0.231	47.1	49.2	0.4–1.0	4.9	5.0
RR new	0.152	0.162	43.8	46.7	0.7–1.0	0.4	0.93
RR cycled	0.172	0.197	49.5	56.7	0.9–1.3	5.0	10.8
PB-VKI[b]	0.234	0.291	54.1	67.2	0.3–1.0	6.2	25.4
PB-VKI cycled	0.288	0.337	66.5	77.8	1.2–3.0	4.4	26.6
SHI-3 cycled	0.201	0.228	36.6	41.5	0.6–1.5	4.2	7.0
SHI-4[b]	0.229	0.243	41.7	44.2	0.2–0.4	5.3	9.0
SHI-4 cycled	0.278	0.338	50.6	61.5	0.7–1.5	4.1	8.5

[a]Calculated from dimensions and weight of the collector and of the electrode.
[b]At the beginning of cycling.

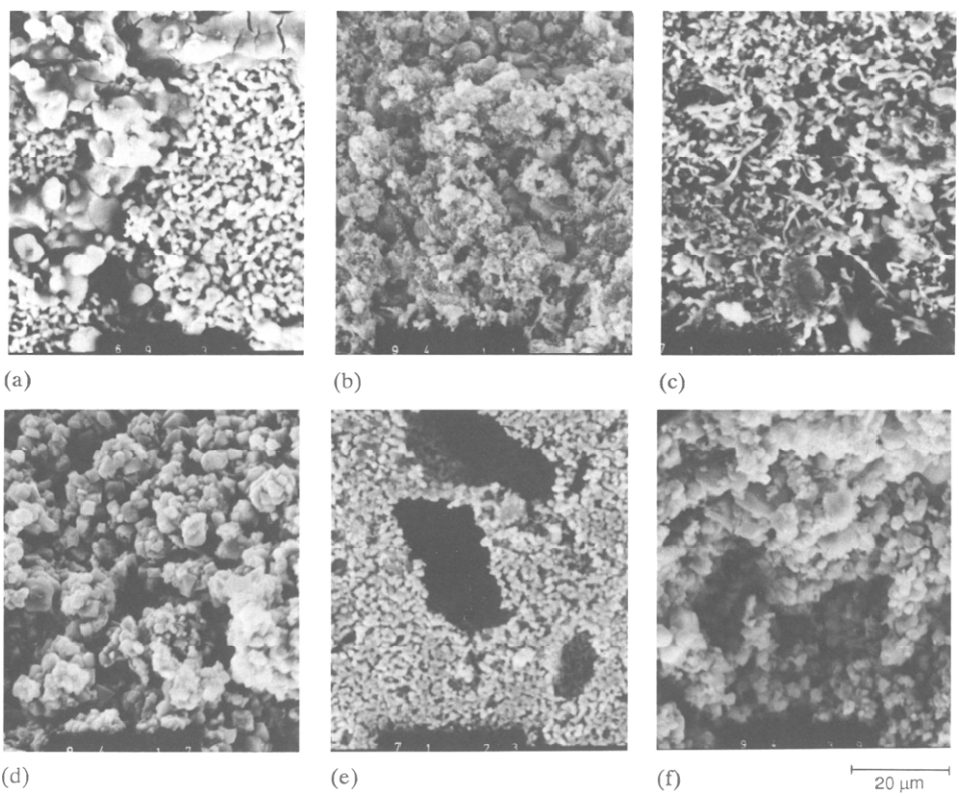

Fig. 6. SEM microphotographs of porous iron electrodes: (a), (c), (e) before cycling; (b), (d), (f) after cycling; (a), (b) electrodes SS; (c), (d) electrodes RR; (e), (f) electrodes SHI.

nonporous, partially-cracked layer (visible at a larger magnification). It seems that the double structure is favourable to sintering, preventing appreciable contraction and formation of visible cracks at the elevated temperature used (785 °C) [5]. During cycling, the larger pores became gradually filled with crystals. The double structure disappeared after cycling, resulting in a uniform, porous structure containing crystals of several μm in size (Fig. 6(b)). The appearance of crystals in the larger pores is in agreement with the dissolution/precipitation mechanism of the iron electrode [27].

The structure of electrode RR is different because the active-material particles before cycling resemble short fibres of various shapes (Fig. 6(c)), which apparently enable the preparation of electrodes by rolling without binder. Cycling results again in the formation of crystals (Fig. 6(d)).

The structure of electrodes SHI prepared from the Bayferrox material is similar to that of electrodes SS except for the cavities of 20 to 40 μm in size left after the removal of the NaCl particles (Fig. 6(e)). The cavities become gradually clogged during cycling (Fig. 6(f)). The electrode SHI-3 has a uniform structure, since in this case the pore-forming substance was the oxide Bayferrox. The structure of electrode SHI-4 was similar to that of SHI-2.

The structure of the PB-VKI electrode was very disordered owing to the bonding material used, which prevented the formation of a quasi-homogeneous mixture.

On the whole, it can be concluded that sintered electrodes are subject to recrystallization during cycling, resulting in the formation of a porous structure that is almost the same in all cases under study.

Conclusions

Voltammograms of sintered iron electrodes show two anodic and two cathodic peaks resembling to those obtained on smooth electrodes. The separation of the potentials of the H_2 evolution and of the Fe(II) reduction is better on sintered electrodes, which have therefore a higher charging efficiency than the nonsintered ones. The self-discharge of the iron electrodes could not be eliminated; it amounts to 4–8% per day. Cyclic voltammetry was proposed as a rapid method for judging the stability of the electrodes and, thus, their cycle life.

Acknowledgement

The authors are indebted to Dr Z. Zábranský of the J. Heyrovský Institute for efficient help in preparing the iron sponge and sintering of the electrodes.

References

1 C. Chakkaravarthy, P. Periasamy, S. Jegannathan and K. I. Vasu, *J. Power Sources, 35* (1991) 21.
2 K. Vijayamohanan, T. S. Balasubramanian and A. K. Shukla, *J. Power Sources, 34* (1991) 269.
3 A. M. Kannan and A. K. Shukla, *J. Power Sources, 35* (1991) 113.
4 O. Lindström, *US Patent No. 3 802 878* (1973).
5 B. Andersson, L. I. Carlsson, R. Christer and R. Johnson, *US Patent No. 4 109 060* (1978).

6 B. Andersson and L. Öjefors, in J. Thompson (ed.), *Power Sources 7,* Academic Press, London, 1979, p. 329.
7 B. Andersson, L. Öjefors and R. Hudson, in J. Thompson (ed.), *Power Sources 8,* Academic Press, London, 1981, p. 379.
8 A. Oliapuram, *US Patent No. 4 335 192* (1982).
9 T. Mitsumata, Ts. Iwaki and M. Fukuda, *Denki Kagaku oyobi Kogyo Butsuri Kagaku, 53* (1985) 325.
10 T. Mitsumata, M. Mori, K. Takahashi, E. Kitamura and Ts. Iwaki, *Denki Kagaku oyobi Kogyo Butsuri Kagaku, 53* (1985) 417.
11 T. Mitsumata, H. Kawano, I. Matsumoto, N. Yanagihara and Ts. Iwaki, *Denki Kagaku oyobi Kogyo Butsuri Kagaku, 53* (1985) 491.
12 G. P. Kalaignan, V. S. Muralidharan and K. I. Vasu, *J. Appl. Electrochem., 17* (1987) 1083.
13 V. S. Muralidharan, M. Ramakrishnan, G. P. Kalaignan, K. Gopalakrishnan and K. I. Vasu, *J. Power Sources, 27* (1989) 311.
14 N. Jayalakshmi and V. S. Muralidharan, *J. Power Sources, 32* (1990) 277, 341.
15 W. A. Bryant, *J. Electrochem. Soc., 126* (1979) 1899.
16 J. Černý, *Ph.D. Thesis*, J. Heyrovský Institute of Physical Chemistry and Electrochemistry, Czechoslovak Academy of Sciences, Prague, 1989.
17 Ju. I. Khimanin, personal communication (1989).
18 M. Cenek and B. Wilczek, *Czech AO No. 248 152* (1986).
19 K. Micka and Z. Zabranský, *J. Power Sources, 19* (1987) 315.
20 B. Andersson and L. Öjefors, *J. Electrochem. Soc., 123* (1976) 824.
21 J. Černý and K. Micka, *J. Power Sources, 25* (1989) 111.
22 L. Öjefors, *Electrochim. Acta, 21* (1976) 263.
23 T. Mitsumata and Ts. Iwaki, *Denki Kagaku oyobi Kogyo Butsuri Kagaku, 53* (1985) 413.
24 J. R. Pierson, C. E. Weinlein and C. E. Wright, in D. H. Collins (ed.), *Power Sources 5*, Academic Press, London, 1975, p. 97.
25 J. Černý and P. Havlík, unpublished results.
26 K. Vijayamohanan, A. K. Shukla and S. Sathyanarayana, *J. Power Sources, 32* (1990) 329.
27 L. Öjefors, *J. Electrochem. Soc., 123* (1976) 1691.